Analysis & Characterization of a Flow Thermo-electrochemical Cell for Power Generation & Heat Convection

by

Ali Sina Booeshaghi

Submitted to the Department of Mechanical Engineering
in partial fulfillment of the requirements for the degree of

Bachelor of Science in Mechanical Engineering

at the

MASSACHUSETTS INSTITUTE OF TECHNOLOGY

June 2017

Signature redacted

Author ....
Department of Mechanical Engineering
May 12, 2017

Signature redacted

Certified by .....
Evelyn N. Wang
Gail E. Kendall Associate Professor of Mechanical Engineering
Thesis Supervisor

Signature redacted

Accepted by .....
Rohit Karnik
Associate Professor of Mechanical Engineering, Undergraduate Officer

Analysis & Characterization of a Flow Thermo-electrochemical Cell for Power Generation & Heat Convection

by

Ali Sina Booeshaghi

Submitted to the Department of Mechanical Engineering
on May 12, 2017, in partial fulfillment of the
requirements for the degree of
Bachelor of Science in Mechanical Engineering

Abstract

In this thesis, I analyzed and characterized a new flow thermo-electrochemical cell that generates power from waste-heat, while in parallel convecting this heat away from the source. I also reviewed previous research on the topic of thermo-electric energy generation, governing physics behind thermo-electrochemical energy generation, actual device fabrication, device testing, results, and applications of this technology.

Thermo-electric devices (TE devices) exhibit the thermo-electric effect, where temperature gradients and material properties work in tandem to drive electron transfer at electrode surfaces, thereby generating electricity. For example, a typical sold-state TE device such as a bismuth telluride TE device, can generate up to 0.300 mV/K [31]. New reseach has emerged [25, 26, 14] focusing on liquid-based thermo-electrochemical (TEC) cells that take advantage of the temperature dependence of oxidation/reduction chemical reactions to generate electricity. One of the major benefits of these TEC devices over traditional TE devices is a much higher $S_e = 1.5$ mV/K; another is the low cost of manufacturing, making them promising for commercial applications.

The new TEC device that I fabricated and studied utilizes a flowing electrolyte instead of a stationary electrolyte. With this new configuration, and a heated boundary condition, I studied both the energy generation and convective heat transfer capabilities of the flowing electrolyte TEC cell. Numerically I obtained a maximum power output and heat transfer coefficient for the TEC cell of $P_{max} = 2.6$ μW and $h = 340$ W/m^{2}K which corroborates well with the experimentally found value of $P_{max} = 2.0$ μW and $h = 450$ W/m$^2\cdot$ K.

If employed in data centers, as a device for CPU cooling, with the given power output I found that a 100,000 ft^2 data center can generate about 21.96 MWh of energy, which at a cost of 0.20 \$/kWh can save a data center about 5,000 \$/year. More generally, the application of this technology in locations where waste-heat is prevalent, will allow for energy recycling and consequent cost savings.

Thesis Supervisor: Evelyn N. Wang
Title: Gail E. Kendall Associate Professor of Mechanical Engineering

Acknowledgments

The author would like to acknoledge Professor Evelyn Wang for her guidance, Professor Baratunde Cola for his support and ideas, Ali H. Kazim for the collaboration, Heena Mutha for her suggestions, Solomon Adera for his mentorship, and his parents for unconditional love and support.

Contents

List of Figures

List of Tables

Chapter 1

Introduction

Waste-heat is a by-product of all energy conversion mechanisms. Of the various grades, low-grade waste-heat (characterized by a temperature less than 230°C) is the most ubiquitous and at the same time most difficult to recover due to challenges such as material limitation, sizing issues, and finding end use for recovered heat [2]. One such source of low-grade waste-heat is the human body that maintains a temperature of 37°C which results in a Carnot efficiency of 5.5%, with the environment, and heat loss of 100 W during normal routine activity [30]. A second source of waste-heat is the ocean. Oceans provide a tremendous reservoir of thermal energy, forming the world's largest source of solar energy collection and storage. If only 0.1% of its thermal energy its utilized and converted to electricity, an ocean could produce 20 times the total electricity consumption in the United States [1]. There are numerous low-grade heat sources where we can employ thermoelectric energy conversion technology in order to unlock a new avenue for energy recycling processes.

A known technique for harvesting usable electrical energy from thermal energy is thermoelectric (TE) energy generation. TE devices employ the thermoelectric effect, where a combination of material properties and thermal gradients, force electron flow resulting in the generation of electricity [24]. TE devices are present in many places from thermocouples to solar energy generators [32], although they are sometimes found in their reverse configuation, as Peltier devices whereby an electrical input produces a temperature gradient as in certain refrigeration devices. However the material constraints, cost-effectiveness, low effiiciencies, and reliability of TE's motivate new attempts [33] to produce improved and more efficient alternatives.

One such novel alternative is an inexpensive liquid-based thermo-electrochemical (TEC) cell [14], [12], [11], that takes advantage of the temperature dependence of electrochemical redox potentials to transfer electrons and produce electric power. Prescribed temperature differences drive electron transfer to and from ions, in an electrolytic solution, to and from electrode surfaces, generating electricity. These lower cost, higher Seebeck coefficient liquid-based TEC devices, commercially viable and higher power output devices can be developed and employed in locations where waste-heat is typically rejected to the environment.

The focus of this work is to develop and understand a flowing electrolyte TEC device that both converts thermal energy into electrical energy while, in parallel, providing thermoregulation to devices that emit waste-heat, in the form of liquid cooling.

Chapter two gives a theoretical perspective on TEC devices, starting first with a brief analysis of solid-state TE devices and then moving on to an indepth analysis of the coupled equations that describe the thermodynamics and electrodyanmics of a TEC device.

Chapter three describes the design, manufacturing, and experimental setup of the TEC device, including electrolyte preparation. as well as the computational domain that was used to run numerical analysis.

Chapter four presents the computational domain that was used to run numerical analysis, the numerical and experimental results as well as a discussion and comparison of the two.

Chapter five comments on applications of this reseach and suggests future directions and device improvements to increase the power output and cooling power of flowing electrolyte TEC device.

1.1 Application for Energy Generation Devices

The United States is home to up to 12 million servers which consume, at an annual rate, 91 billion kWh [3]. This is enough to power all of the homes in New York City for a two years. It is projected that by 2020, that number could increase to 140 billion kWh annually. Keeping these data centers cool is no simple task; with power densities of up to 578.7 kW/m^2 and expelled heat of a temperature less than 230°C, the waste-heat that must be removed consumes massive amounts of electricity. Typically half of the energy consumed in data centers is used to provide cooling

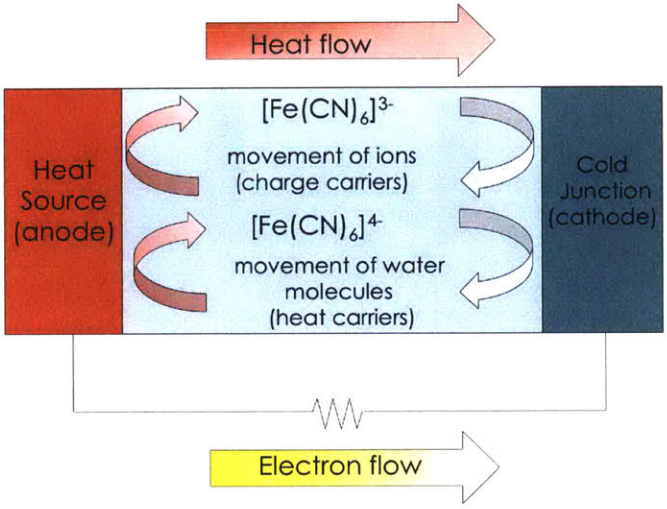

Figure 1-1: An example of a sTEC where charge migration is limited to diffusion and natural convection. The $Fe(CN)_6{}^{3-}$ ion gets reduces at the cold electrode and becomes $Fe(CN)_6{}^{4-}$ then this ion gets oxidized at the hot electrode and returns to $Fe(CN)_6{}^{3-}$.

to these CPUs in order to avoid catastrophic electrical component failure. In an attempt to alleviate the low efficiencies of cooling technologies, liquid cooling has emerged as a viable method [19, 34, 4]. The need for liquid cooling is ever present if we are to keep up with Moore's law.

With a clear source of underutilized thermal energy, Data Centers show promise as energy generation centers, whereby the recycled electrical energy can be used to power the facilities, thereby aiding in reducing our carbon footprint [29, 5].

1.2 Thermo-electrochemical Cells

TEC cells are the chemical analog of TE cells, however their chemical nature means that the resulting thermodynamics and electrodynamics are more complicated. Charge is transfered by migration of ions in an electrolyte, for TEC cells, whereas electrons move between holes in TE cells. More specifically, temperature differences in TEC cells thermodynamically drive oxidation/reduction reactions at electrode surfaces, resulting in a voltage, current, and power output.

Stationary TEC Cells

Stationary TEC (sTEC) cells are the most common type of TEC cells studied, and have been researched since 1880 [7] and reviewed extensively by [23] and more recently by [11]. The main char-

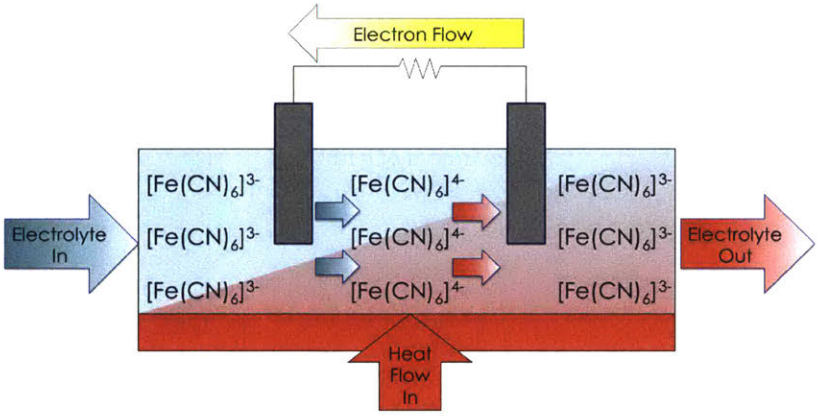

Figure 1-2: An example of a fTEC where charge migration is assisted by forced convection. The $Fe(CN)_6{}^{3-}$ ion gets reduces at the cold electrode, gets convected to the and in the process heated by the boundary condition and then becomes $Fe(CN)_6{}^{4-}$.

acteristics of a sTEC cell is the prescribed temperature difference between electrodes and charge migration being limited to diffusion and natural convection. An example can be seen in **fig. 1-1**.

Quickenden *et al.* 1995 were interested in determining the conversion efficienies for sTEC cells for use in solar energy conversion. They found that of the best power conversion efficiency (relative to that of a Carnot engine operating between the same T_h and T_c temperatures) and thermoelectric coefficient was $\eta_r = 0.5\%$ and $S_e = 1.5$ mV/K respectively, and that it would be difficult to obtain values over $\eta_r = 1.2\%$. The oxidation/reduction couple that they found resulted in in the highest η_r and S_e was $Fe(CN)_6{}^{3-}/Fe(CN)_6{}^{4-}$. More importantly, they found that these efficiencies are smaller than that for metal and semiconductor thermocouples ($\eta_r = 48.0\%$ and $S_e = 1$ mV/K) due to the high concentration of water molecules which conduct heat but which do not act as charge charriers.

Gunawan *et al.* 2013 reports that of the articles reviewed, [14] and [15] showed the highest $\eta_r = 1.4\%$ for a $Fe(CN)_6{}^{3-}/Fe(CN)_6{}^{4-}$ redox system using nanostructured electrode materials. Further advances in electrode material selection find that higher surface area electrodes, such as carbon nanotubes, result in a higher specific power output compared to lower surface area materials [15]. Also, lower tortuosity materials are desirable for high electrical conductivities.

The biggest drawback of sTEC cells is that charge transfer is limited to diffusion and natural convection. A result of this is an ionic boundary layer surrounding the electrode surfaces, where ions are "trapped", that raises the ohmic resistance of the cell, or the resistance that opposes charge

transfer within the electrolyte from one electrode to another.

Flowing TEC Cells

Flowing TEC (fTEC) cells exhibit similar characteristics to sTEC cells. The main difference is that in fTEC cells, the electrolyte flows from one electrode to the other by forced convection and there is a prescribed temperature boundary condition to the base of the cell, **fig. 1-2**. From this modification, two effects emerge: convective liquid cooling and forced convection charge migration. Convective liquid cooling dictates the temperature difference between electrodes based off of the fluid properties and its flow rate. This is starkly different than the prescribed temperature difference that sTEC cells employ. Forced convection charge migration helps to remove the ionic boundary layer that surrounds an electrode thus lowering high ohmic resistance that plagues sTEC cells.

Chapter 2

Governing Physics

In the following sections reviewed the governing physics of each phenomena involved in TEC cell operation. First I will qualitatively discussed the phenomena and then I supported that discussion by presenting the mathematics that quantifies each effect.

2.1 Thermo-electric Effect

The thermoelectric effect, discovered in 1821 by Thomas Johann Seebeck [27], is a link that connects heat and electricity. The effect quantifies how temperature gradient inputs result in voltage outputs. It is employed in a variety of applications from solid-state heat engines to thermocouples. Its mechanism is quite simple, by adding heat to one end of a TE material, an electromotive force is generated. This electromotive force can be thought of as a force that drives negatively charged particles, electrons, from areas of high electric potential to low electric potential. This is a result of the thermal energy that was added to one end of a TE material. As the heat diffuses into the material, the electric potential lowers, thus lowering the amount of electron flow. As such, TE materials with a high electrical conductivity and a low thermal conductivity are desirable.

The thermoelectric effect, also known as the Seebeck Effect, is an observable property of various metals and chemical solutions and is defined in the following way relating the induced electromotive force E_{emf} to the Seebeck coefficient, S_e, by the application of a temperature gradient

∇T:

$$E_{\text{emf}} = -S_e \nabla T. \tag{2.1}$$

Given a static electric field within a TE material, $E_s = -\nabla V$, the total electromotive force is expressed as a sum of the electric fields $E = E_s + E_{\text{emf}}$. We can then use Ohm's law, $J = \sigma E$ to express current density, J, as a function of E and the material's electrical conductivity, σ:

$$J = \sigma \left(-\nabla V - S \nabla T\right). \tag{2.2}$$

The Seebeck Coefficient is then defined for the case when $J = 0$ or more qualitatively when the system has an open circuit,

$$S_e = -\frac{\nabla V}{\nabla T}. \tag{2.3}$$

The Seebeck coefficient of TE materials can be found experimentally by using a temperature source and a temperature sink and then determining the voltage output of the material. In measuring the Seebeck coefficient, careful attention must be paid to the location of the heaters, thermocouples, and voltage probes. Older techniques utilize a potentiometer [10] and heated copper plates to determine the Seebeck Coefficient and newer methods use 4-point thermocouple and voltage probe measurement techniques [6], an example is shown in **fig. 2-1**. Typical Seebeck coefficients for common TE materials are shown in **table 2.1**.

Thermo-electric Material	Dopant/Counterion	Seebeck Coefficient [μV/K]
polyacetylene	I_2	15
PBTTT	FTS	33
PEDOT	ToS + TDAE	215
PEDOT	PSS (with Te nanowires)	163

Table 2.1: A list of Seebeck Coefficients for different TE materials, [18].

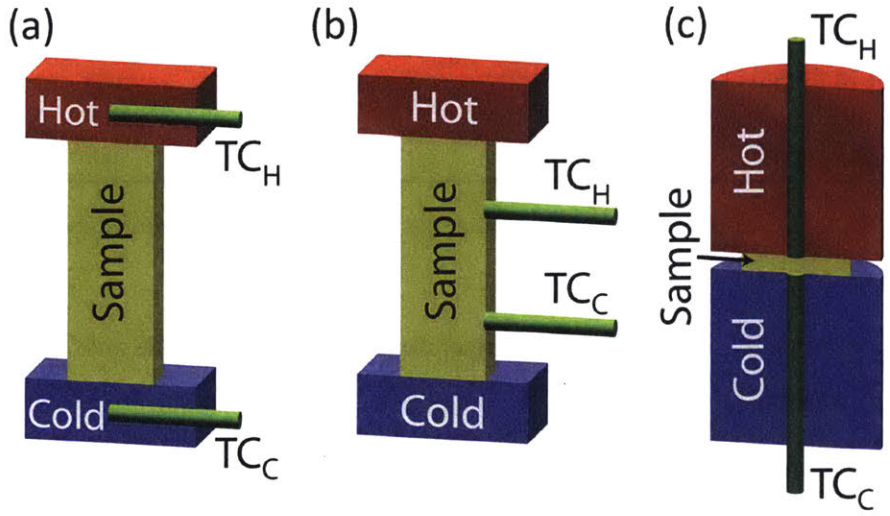

Figure 2-1: Borup *et al.* shows different configurations for measuring the Seebeck coefficient of TE materials. (a) 2-point, (b) off-axis 4-point, and (c) on-axis 4-point.

2.2 Thermo-electric Cells (TE Cells)

A solid-state thermo-electric cell is a traditional TE conversion device where an applied temperature difference between P and N type materials results in electron flow and electricity generation [28]. A typical bismuth telluride solid-state TE cell has a Seebeck coefficient of up to 230 μV/K [22]. However, this material property does not paint a complete image of a TE cell. As mentioned in **section 2.1** the electrical and thermal conductivities of a TE material can influence its effectivness as a TE device. Therefore in order to better understand the viability of TE cells, a figure known as the TE figure of merit, is typically used and is defined as:

$$ZT = \frac{S_e^2 \sigma}{\kappa} T, \tag{2.4}$$

where σ is the electrical conductivity, κ the thermal conductivity, S_e the Seebeck Coefficient of the material, and T the absolute temperature at which the properties are measured [24]. Common ZT values range from 0.5-2.0 [20] with commercially viable TE devices having a $ZT \approx 1$ [8]. With this figure of merit we can calculate device efficiency [16]:

$$\eta_{max} = \frac{T_h - T_c}{T_h} \cdot \frac{\sqrt{1 + Z \cdot T_{avg}} - 1}{\sqrt{1 + Z \cdot T_{avg}} + \frac{T_c}{T_h}}. \tag{2.5}$$

Electrolyte	Electrode Material	Seebeck Coefficient [mV/K]
0.1 M $Fe(CN)_6^{3-/4-}$	SWCNT	1.43
0.01 M $CuSO_4$+0.1 M H_2SO_4	Cu	0.63
0.4 M $I^-/I_3^- + H_2O$	Pt	0.3
0.4 M $Fe(CN)_6^{3-/4-}$	Pt	1.4

Table 2.2: A list of Seebeck Coefficients for different TEC electrolytes, [11].

where $T_{avg} = (T_h + T_c)/2$, and T_c is the temperature at the cold electrode and T_h the temperature at the hot electrode.

In an effort to maximize the voltage output, ZT, and power output, and to overcome the material constraints, cost-ineffectiveness, and lack of reliability of current thermoelectric cells, new attempts have been made to produce improved alternatives that focus on higher Seebeck coefficient materials.

2.3 Thermo-electrochemical Cells (TEC Cells)

These new alternatives are TEC cells which, unlike TE cells, utilize electrochemical oxidation/reduction reactions that exhibit the TE effect, i.e. temperature dependent voltage generation. The benefits of these new alternatives are higher Seebeck coefficients, **table 2.2.**

TEC cells work in the following manner: the electrolyte within the cell undergoes a thermally driven oxidation/reduction reaction that results in power generation at electrode surfaces. There are two types of TEC cells one with a stationary electrolyte (sTEC cell) **fig. 1-1**, and one with a flowing electrolyte (fTEC cell) **fig. 1-2**. Both operate under the same principle of thermally driven oxidation/reduction reactions. The specific electrolyte I used for this thesis was an equimolar solution of a $Fe(CN)_6^{3-}/Fe(CN)_6^{4-}$ redox couple where the thermodynamics and electrodynamics follow the reversible redox chemical reaction:

$$Fe(CN)_6^{3-} + e^- \longleftrightarrow Fe(CN)_6^{4-}, \qquad E_0 = +0.356\ \text{V}. \tag{2.6}$$

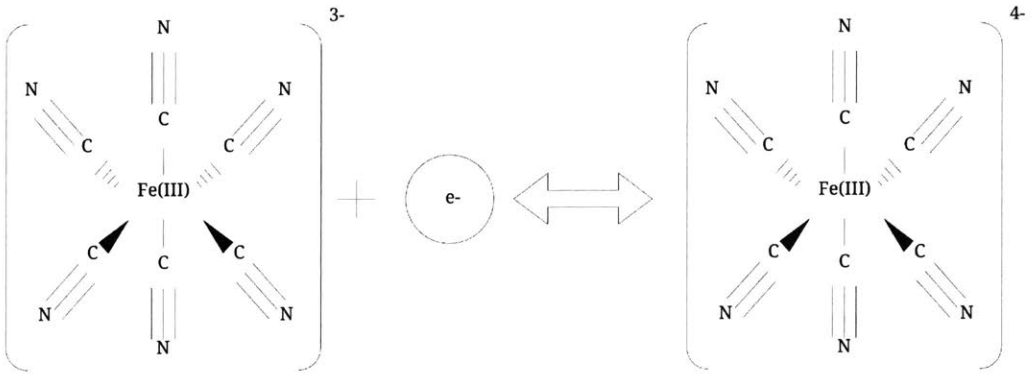

Figure 2-2: The transition-metal complex of an Fe^{3+} ion bounded to six CN^- ligands that reduce (gain an electron) to create another transition-metal complex of Fe^{2+} bounded to six CN^- ligands, all in an octahedral geometry.

2.3.1 Electrodynamics

We first turn our attention to the molecular level in our study of the $Fe(CN)_6{}^{3-}$ / $Fe(CN)_6{}^{4-}$ redox system so that we may better understand electron movement. These ions initially start out as potassium salts which were dissolved in deionized water. What is left in the beaker upon the dissolution of these salts are transition-metal complexes, namely an $Fe^{2+/3+}$ ion surrounded by CN^- ligands in an octahedral geometry [9], **fig. 2-2**.

When the oxidation/reduction reaction takes place, the electron moves into one of the five d-orbitals of the Fe^{3+} ion, turning it into an Fe^{2+} ion. Crystal field theory [9] gives us a picture as to the location of this new electron, **fig. 2-3**. Fe^{3+} binded to six CN^- ligands, gets reduced in a half-reaction at the first electrode to Fe^{2+} binded to six CN^- ligands. Fe^{3+} is a d^5 system with five electrons in its d-orbital. The Fe^{3+} ion receives an electron into its t_{2g} d-orbital to become Fe^{2+}. This is a favorable galvanic cell reaction, because the redox potential is positive and as a result the reaction is spontaneous in the forward direction, i.e. its Gibbs free energy ΔG is negative in the forward direction:

$$E_f^0 > 0 \tag{2.7}$$

$$\Delta G_f^o = -nFE_f^0 < 0 \tag{2.8}$$

$$= -34.35 \text{ kJ/mol}, \tag{2.9}$$

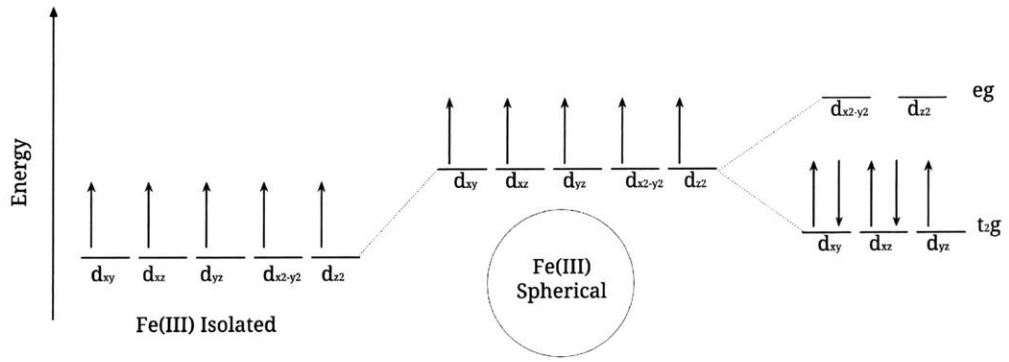

Figure 2-3: A crystal field theory energy diagram for the five d-orbitals of the Fe^{3+} ion. The incoming electron will be placed in the d_{yz} orbital since electrons want to occupy the lowest energy state available.

where $n = 1$ is the number of electrons transferred in the reaction, and $F = 96485$ C/mol is Faraday's constant.

Now that we have a pretty clear picture of the forward reaction, we must consider the backwards reaction, i.e. the oxidation half-reaction of Fe^{2+} back to Fe^{3+}, where an electron is liberated from the t_{2g} d-orbital and transferred to an external circuit. This is not a favorable reaction under standard conditions since the backwards reaction has a negative reduction potential, $E_b^0 < 0$. This implies that the reaction is not spontaneous in the backward direction, i.e. $\Delta G_b^0 = -\Delta G_f^0 > 0$. However, the reaction we are studying is not under standard conditions. If we were to heat up the electrolyte containing these ions, then the oxidation half-reaction would become spontaneous in the backwards direction since we would be changing the Gibbs Free energy:

$$\Delta G_b = \Delta G_b^0 + RT \ln\left(\frac{[\mathrm{Fe(CN)}_6^{3-}]}{[\mathrm{Fe(CN)}_6^{4-}]}\right). \tag{2.10}$$

In fact we can raise the temperature just enough to thermally regenerate $Fe(CN)_6^{3-}$ from $Fe(CN)_6^{4-}$, by making the backwards reaction spontaneous, i.e. making $\Delta G_b < 0$. After the forward reaction occurs then we are left with an overabundance of $[Fe(CN)_6^{4-}]$ and almost no $[Fe(CN)_6^{3-}]$. This is enough to make $\Delta G_b < 0$.

This allows us to continually oxidize and reduce the $Fe^{2+/3+}$ ions within the fluid, allowing for continual transport and flow of electrons to an external circuit.

The Nernst equation allows us to calculate the open-circuit voltage we expect to see for a TEC

cell under a prescribed temperature difference between two electrodes,

$$E_b - E_b^\circ = (T_b - T^\circ)\frac{\Delta S_{rx}^\circ}{nF} + \frac{RT}{nF}\ln\left(\frac{[\mathrm{Fe(CN)}_6^{3-}]}{[\mathrm{Fe(CN)}_6^{4-}]}\right) \tag{2.11}$$

$$E_f - E_f^\circ = (T_f - T^\circ)\frac{\Delta S_{rx}^\circ}{nF} + \frac{RT}{nF}\ln\left(\frac{[\mathrm{Fe(CN)}_6^{4-}]}{[\mathrm{Fe(CN)}_6^{3-}]}\right) \tag{2.12}$$

$$V_{oc} = E_b + E_f = \frac{\Delta S_{rx}^\circ (T_b - T_f)}{nF}. \tag{2.13}$$

As seen, in order to maximize the voltage output we either increase the temperature difference between the anode and the cathode or select a material with a higher Seebeck coefficient $S_e = \frac{\Delta S_{rx}^\circ}{nF}$.

I specifically chose $\mathrm{Fe(CN)_6}^{3-}$/ $\mathrm{Fe(CN)_6}^{4-}$ as the oxidation/reduction system due to its high Seebeck Coefficient of ~1.4-1.6 mV/K [13, 21, 17]. This results in a high open-circuit voltage.

Voltage output alone does not paint a complete picture of the system. Power generation is a function of both current and voltage output, and a high power output requires a high voltage and high current output. Current output can be thought of as electron fluxes at the electrodes, both anode and cathode. Fluxes at electrode surfaces result in a buildup of current densities that are determined by the kinetics of the chemical reactions at the electrode i, $i \in \{\text{anode, cathode}\}$ given by the Butler-Volmer equation:

$$j_i = nFK_0 \exp\left[\frac{E_{x_a}}{R}\left(\frac{1}{T_0} - \frac{1}{T_i}\right)\right] \cdot \left[C_o^i \exp\left(\frac{-nF(1-\theta)\xi_i}{RT_i}\right) - C_R^i \exp\left(\frac{nF\theta\xi_i}{RT_i}\right)\right], \tag{2.14}$$

where the n is the number of electrons transferred in the reaction, F is Faraday's constant, K_0 is the reaction rate constant, E_{x_a} is the activation energy for the reaction, R is the ideal gas constant, T_0 is the reference temperature, T_i is the temperature at the i^{th} electrode, θ is a constant determined by the reversibility of the reaction, ξ_i is the overpotential generated by the reaction at the i^{th} electrode, and C_0^i/C_R^i is the oxidized/reduced species concentration at the i^{th} electrode.

With the current output and voltage output, we can now determine the power output:

$$P_{gen} = IV. \tag{2.15}$$

Experimentally, however, the maximum power output takes the form [14]:

$$P_{max} = 0.25 V_{oc} I_{sc}, \tag{2.16}$$

where V_{oc} is the open-circuit voltage and I_{sc} is the short-circuit current.

As mentioned previously, the mass flow of the electrolyte is beneficial, as it would aid in movement of ions. For a typical sTEC cells, ion transport from the anode to the cathode is restricted to natural convection, diffusion and migration. However, in the fTEC cell the forced convection of ions replenishes and removes any already oxidized or reduced ion species at the electrode surface. Unidirectional flow restricts movement of ions backwards and reduces one of the performance-limiting steps in fTEC cells, that of ion transport, to and from electrode surfaces.

2.3.2 Heat Transfer & Fluid Mechanics

We can model the fluid mechanics and heat transfer of the electrolyte using a steady state momentum conservation of a laminar flow with only gravitational forces present. Assuming a no slip condition at the wall ($\vec{u}_{wall} = 0$) we get that

$$(\vec{u} \cdot \nabla)\, \vec{u} = \nu \nabla^2 \vec{u} + \vec{g} \left(\frac{\rho_0 - \rho}{\rho_0} \right). \tag{2.17}$$

where $\vec{u}$ is the velocity field of the fluid, ρ the density of the fluid, ν the viscosity of the fluid, and g gravity. This equation is used in our computational model, and interacts with a thermal module to determine the temperature and velocity field of a flowing electrolyte.

The fluid, in our system, convects heat from the constant temperature heat source. The temperature of our fluid therefore is defined by the unsteady heat conduction equation:

$$\frac{\partial T}{\partial t} = \nabla \cdot (k \nabla T) - \rho\, c_p \nabla \cdot (\vec{u} T) + \vec{Q} \tag{2.18}$$

$$\vec{u} = \langle u, v \rangle \tag{2.19}$$

$$\vec{Q} = \langle 0, 0 \rangle, \tag{2.20}$$

where k is the thermal conductivity of the fluid, T the temperature of the fluid, and $\vec{Q}$ a heat source.

The flow is assumed to be laminar and incompressible, i.e. divergence free ($\nabla \cdot \vec{u} = 0$), with a known velocity profile and a uniform, constant thermal conductivity ($\nabla \cdot k = 0$). We also seek a steady state solution where $\frac{\partial T}{\partial t} = 0$. With these assumptions we get that

$$\rho\, c_p\, \nabla \cdot (\vec{u}\, T) = \rho\, c_p\, (T\, \nabla \cdot \vec{u} + \vec{u}\, \nabla \cdot T) \tag{2.21}$$

$$= \nabla \cdot (k\, \nabla T) + \vec{Q} \tag{2.22}$$

$$= (\nabla \cdot k)\, \nabla T + k \nabla^2 T + \vec{Q} \tag{2.23}$$

The steady state solution for the temperature distribution, which will assist in understanding the power output as a function of the fluid velocity $\vec{u}$ is given below:

$$\rho\, c_p\, \vec{u}\, \nabla \cdot T = k \nabla^2 T + \vec{Q} \tag{2.24}$$

To better pose the above problem, I compared the convection of heat to that of diffusion of heat. Convection occurs in the flow direction and diffusion occurs in the transverse direction. The Peclet gives the ratio of advection of temperature to diffusion of temperature. Since our problem is two-dimensional, the Peclet number must be calculated twice; advection will dominate one dimension and diffusion will dominate the other:

$$Pe_x = \frac{u\, L}{k} \sim 1 \tag{2.25}$$

$$Pe_y = \frac{v\, h}{k} << 1. \tag{2.26}$$

In the flow direction the convection and diffusive of heat are of a similar order whereas in the non-flow direction, the diffusive terms dominates. As a result, we will make a simplifying assumption that advection dominates diffusion, in the flow direction.

Of equal interest to us is the heat transfer coefficient of the fTEC cell as a function of flow rate. Since an fTEC cell can be modeled as a heat exchanger with a constant temperature boundary condition, the heat transfer coefficient can be found by

$$\bar{h} = \frac{\dot{m} c_p}{2wh} \ln\left(\frac{\Delta T_{in}}{\Delta T_{out}}\right) \tag{2.27}$$

where $\dot{m}$ is the mass flow rate of the fluid, $w \cdot h$ is the cross sectional area perpendicular to the flow direction, c_p is the heat capacity of the electrolyte, ΔT_{in} is the temperature difference between the bulk fluid at the inlet and the boundary condition, and ΔT_{out} is the temperature difference between the bulk fluid at the outlet and the boundary condition.

These equations are solved in the COMSOL model to perform the numerical analysis in **chapter 4**.

Chapter 3

Device Fabrication & Experimental Setup

In this chapter we review the design of the fTEC cell, the iterations that the design went through, the fabrication of the device, and the experimental setup.

3.1 Design & Fabrication of the Cell

Prior to fabricating the fTEC cell I first identified that the fTEC cell must follow certain requirements: the cell must be

- leak free,
- thermally conductive,
- compatible with $Fe(CN)_6{}^{3-}/Fe(CN)_6{}^{4-}$ electrolyte,
- capable of in-flow electrode insertion,
- electrically isolating.

In the first iteration of the cell, I was aware of all of the design requirements except for the last one, a flaw in iteration one & two which will be discussed more in **section 4.2**.

For both iteration one & two I used Solidworks & MasterCam to design and create the G-Code for CNC machining. I used the Prototrak Mill in MIT's Hobby shop to machine two iterations of this device out of 6061-T6 aluminum. The designs can be seen in **fig. 3-1a & 3-1b**.

3.1.1 Iteration One

Prior to iteration one of the fTEC cell, I had never done any hardcore CNC machining myself. As such, iteration one can be broken down into two sub-iterations called non-working and working.

The design of iteration one was inspired by common liquid cooling blocks that are mounted to CPU units. These units are marked by a high surface area geometry and high thermal conductivity materials, typically copper. The high surface area allows for more liquid to solid points of heat exchange while the high thermal conductivity of the material assists in transferring heat readily to those points from the heat source. The reason for following this design paradigm is because the fTEC I was designing has an application in the space of CPU cooling whereby the heat released from the CPU chip drives the oxidation reduction/reaction at the electrodes within the fTEC electrolyte thereby generating electricity.

Iteration one has the following design features that were intended to make experimentation simple: NPT tapped holes on the top for electrolyte inlet/outline lines, holes in the top plate along the flow path to allow for easy insertion of graphite electrodes, and a sealing rim around the cell that was filled with sealant to prevent leaks. The machined iteration one can be seen in **fig. 3-3a**. The material is 6061-T6 aluminum a metal that is compatible (unaffected by the corrosive nature of the electrolyte) with the working fluid.

Takeaways from Iteration One

Iteration one has too many variable dimensions and sizes for it to be of any use in scientific inquiry. The spacing between the "channels" was not uniform, and the electrode placements were not consistent. Secondly, the sealing rim did not seal properly resulting in many leaks. With the variable sizes, it was impossible to predict what my flow regime would look like, i.e. is each channel experiencing laminar flow, where I can predict the flow profile with a parabola? This would allow me to better estimate heat transfer within the cell if I were to have this knowledge; hence I made those improvements in iteration two.

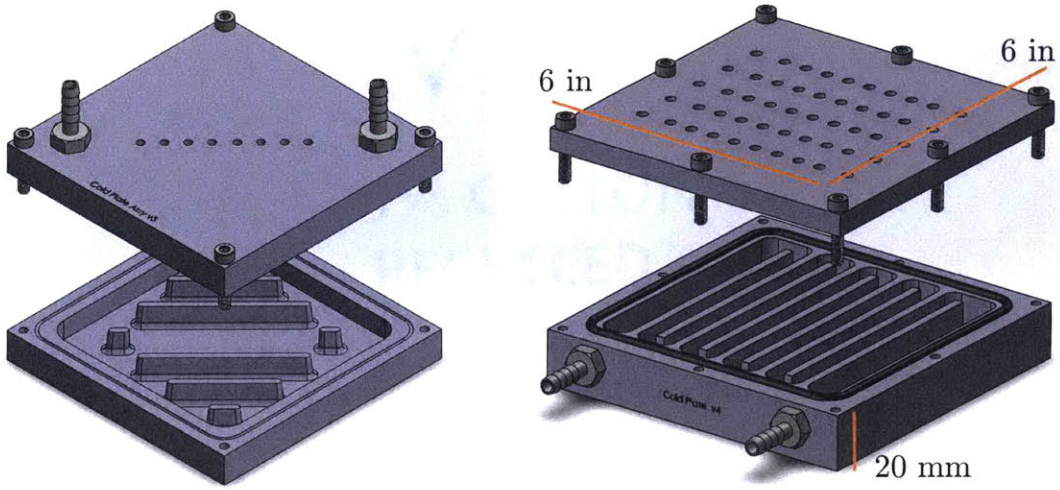

(a) *fTEC Cell Iteration One*

(b) *fTEC Cell Iteration Two*

Figure 3-1: The two iterations of the fTEC cell. From the first iteration of the cell (a) I made design modifications, such as a snaking fluid path, side inlet/outlet holes, and inline electrode holes so that iteration two (b) would provide a more accurate (and cleaner a.k.a. leakproof) function of the cell.

3.1.2 Iteration Two

Iteration two built upon the takeaways from iteration one. I designed the channels to be of constant width, the electrode hole locations to be in a "matrix" form for variable electrode distance testing, and the inlet/outlet lines placed on the side of the cell. The machined iteration two can be seen in **fig. 3-3b**. The issues that arose with iteration two are quite different than those from iteration one and only arose due to testing the experimental setup.

For each hole in the top plate of the cell, I needed to insert both a thermocouple and a graphite electrode (for reasons that are discussed in **section 3.3**). Ensuring that I could insert both the electrode and the thermocouple, while also ensuring that the device was leakproof during operation, was a beast of its own. Initially, I attempted to wrap both the thermocouple and graphite electrode in heatshrink tubing to create a compliant seal when inserted into the top plate. This did not prevent any leaks. To combat this, I spread RTV gasket sealer all over the electrode hole but nonetheless leaks persisted.

After dealing with the leaking issue for a while, I finally stumbled across a chemically resistant nylon multi-cord grip, **fig. 3-2**. One end of the cord-grip is NPT threaded so that I could NPT tap into the top plate and use teflon tape to create a seal. This solution worked well.

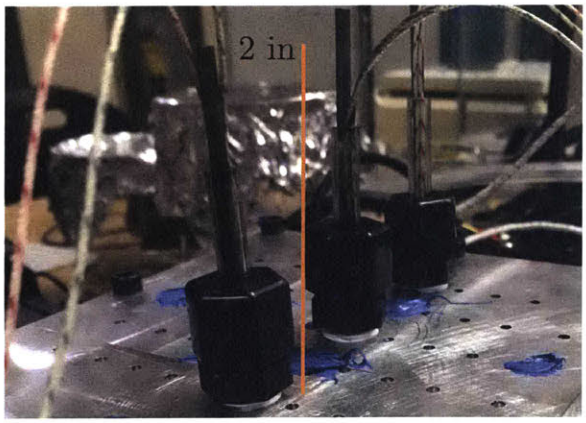

Figure 3-2: The multi-cord nylon seal with NPT thread was threaded into the top plate to prevent leaks for the electrode and thermocouple probes.

3.2 Electrolyte Preparation

The working fluid for my experiments was an equimolar solution of $Fe(CN)_6{}^{3-}/Fe(CN)_6{}^{4-}$. At 0.4 M, the solution is at its highest possible redox couple concentration, but still low enough to avoid electrolyte degradation at high concentrations [15], allowing me to maximize the kinetics of the chemical reaction, resulting in an increased current output.

Since I desired a 0.4 M solution, utilizing a 750 mL container, I needed 0.3 moles of total solute. The solution should be equimolar $K_3(FeCN)_6 = 329.24$ g/mol and $K_4(FeCN)_6 = 422.39$ g/mol, therefore we need 0.15 moles of each solute. This results in a mass of $K_3(FeCN)_6 = 49.39$ g and a mass of $K_4(FeCN)_6 = 63.36$ g to be dissolved in a 750mL container of deionized water to create a 0.4 M solution.

3.3 Experimental Setup

The purpose of these experiments was to determine how the fTEC cell functions, i.e. what is its power/voltage/current outputs and heat trasnfer coefficient, at different flow rates. **Fig. 3-4** shows a global diagram for the experimental setup that guided the physical setup for the experiment. Fluid is pumped from a resevoir, into the fTEC cell where it is heated. The heat drives an oxidation reduction reaction at the electrodes thereby generating electricity. Then the fluid leaves the fTEC cell and cycles back into the reservoir. For these experiments, a closed-loop fluid system was desirable for easy operation and testing. The difference between a closed-loop and open-loop

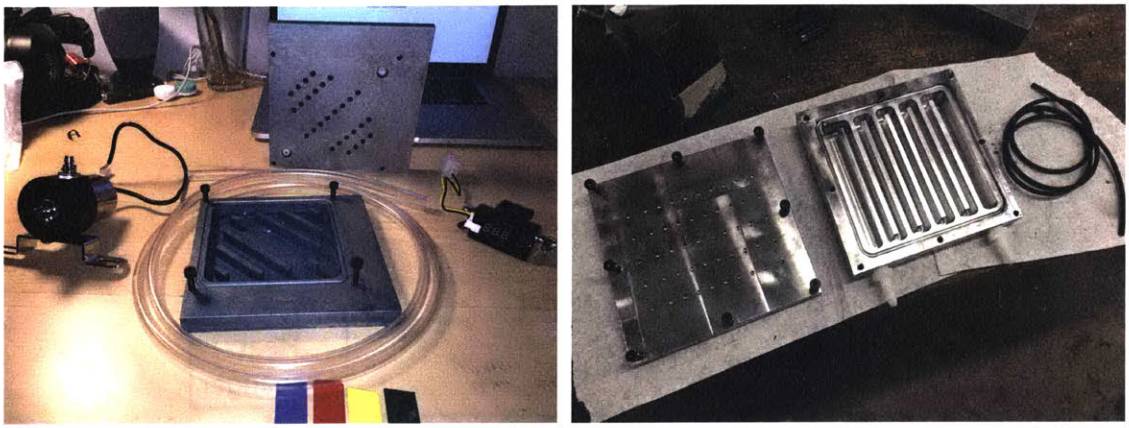

(a) *Fabricated Iteration One* (b) *Fabricated Iteration Two*

Figure 3-3: The two iterations of the fTEC cell after they have been machined. The main difference between iteration one (a) and iteration two (b) are a longer flow path, smaller channels, and variable 2D electrode placement.

fluidic system is that in the closed loop, the fluid passes through the fTEC cell (after having undergone an increase in temperature) and then has its excess heat dissipated through an external heat exchanger before returning to the fluid reservoir.

The main parameters of interest in the system are the flow rate, the temperature of the fluid at the electrodes, and the voltage/current output at the electrodes for a given electrode distance. To set the flow rate, I used a Cole-Parmer peristaltic pump. I used in-line K-type thermocouples at the electrode locations and a temperature probe in the reservoir bath to monitor fluid inlet temperature and temperature at the electrodes. The voltage and current outputs were measured using a potentiostat.

The purpose of each experiment was to determine the tempererature difference, heat transfer coefficient, open-circuit voltage, and current output between two in-line electrodes, as a function of flow rate. This will allow me to determine the power generation capabilities of the fTEC cell as well as its effectivness at heat removal from a heat source. For each experiment, I ensured that the the heater was at a constant temperature of 400 K and I let the peristaltic pump run for some time until the fluid reached a steady-state outlet temperature. Experimentally, the steady-state point was characterized by no temperature increase of the fluid after two minutes of operation. This operation only needed to be performed once per testing "session." Two iterations of my experimental setup can be seen in **fig. 3-5a & 3-5b**.

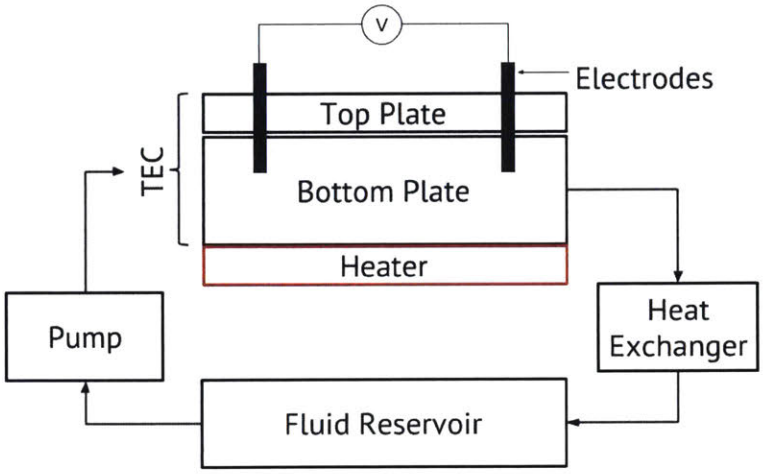

Figure 3-4: A schematic of the experimental setup. Electrolyte gets pumped to the fTEC cell by a peristaltic pump, the heater heats the electrolyte which consequently reacts at the electrode surfaces, generating a voltage. The system is closed loop, with the fluid resevoir maintained at a constant temperature.

Once steady-state was reached, I turned on the potentiostat and ran two methods: an open-circuit voltage method, and a chronoamperometry method. The open-circuit voltage method would measure the open-circuit voltage for three minutes, which should correspond to the temperature difference I recorded by a handheld thermocouple meter multiplied by the Seebeck coefficient of the electrolyte. The second method I ran was a chronoamperometry method which logged the short-circuit current over time. With the open-circuit voltage V_{oc} and the short-circuit current I_{sc}, I was able to calculate the maximum experimental power of the device by

$$P_{max} = 0.25\, I_{sc} V_{oc}. \tag{3.1}$$

With regard to material selection, it is important to note that the corrosiveness of the electrolyte was a limiting factor. The chemical compatibility between the electrolyte and 6061-T6 aluminum proved to be moderate and suitable for this experiment. All connectors are NPT with chemically inert rubber tubing connecting the components of the system.

(a) *Experimental Setup Iteration One* (b) *Experimental Setup Iteration Two*

Figure 3-5: The two iterations of the experimental setup for the fTEC Cell. The main difference between iteration one (a) and iteration two (b) are that the second iteration paid more careful attention to monitoring all variables in the system, one example is having a constant temperature bath for the inlet electrolyte.

3.3.1 Electrode Selection

For the electrode material, I utilized extruded graphite. Studies have been conducted on different electrode materials, such as carbon nanotubes for their high surface area. Graphite was chosen as the electrode material for its thermodynamic stability [11]. The electrodes were inserted into the top plate of the device, electrically isolated from the cell, and connected to a potentiostat.

Chapter 4

Device Performance

The fTEC cell that I built was characterized by its ability to convect heat and its ability to generate power. These two properties of the cell are at odds with each other, since at lower flow rates I observed a higher power output but a lower heat transfer coefficient but for a higher flow rate, I observed a lower power output and a higher heat transfer coefficient. In order to validate these observations I evaluated the fTEC cell using numerical simulations and experiments. The numerical simulations were performed with COMSOL.

4.1 Numerical Analysis

The COMSOL analysis of the fTEC cell involved creating a two dimensional domain and then solving the multiphysics equations specified in **section 2.3**.

4.1.1 Domain Setup

I wanted to simplify my three dimensional fTEC cell to a tractable two dimensional system for numerical analysis. To this end, I decided to take a "differential" element of my fTEC cell, i.e. a side view of the flow channel bounded on each end, spatially, by two electrodes. The domain can be seen in **fig. 4-1**. The electrolyte enters from the left hand side of the element, is exposed to a constant temperature boundary condition, undergoes thermally driven oxidation/reduction reactions and then exits the cell on the left side.

Within COMSOL I used the heat transfer, fluid mechanics, and electrochemistry modules to

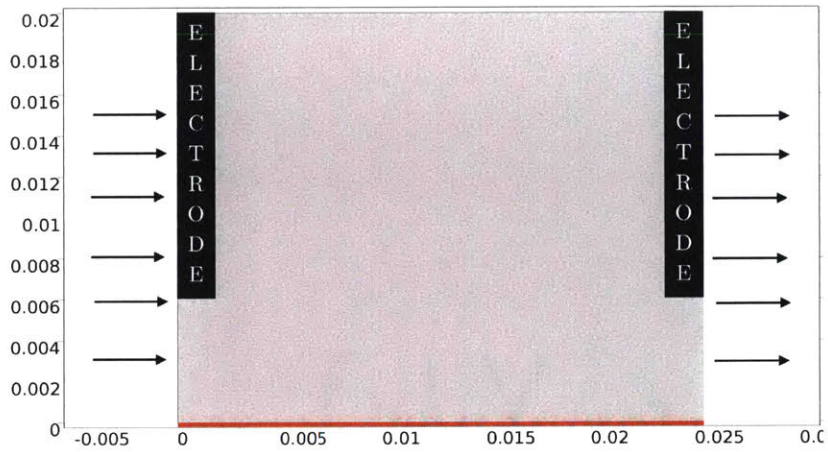

Figure 4-1: The "differential" domain for my numerical analysis. The electrolyte flows in from the left, into the element, is exposed to a constant temperature boundary condition, oxidizes and reduces at the electrodes, and then exits the element.

solve the multiphysics problem. I sought a steady-state solution to the problem: electrolyte enters the left side of the element at equimolar concentrations, the ions reduce at the first electrode, undergo a temperature increase by the constant temperature boundary condition, and then oxidizes at the outlet electrode.

Specifically, the assumptions and geometry of the model are as follows:

- the cell measures 2.54 cm $\times$ 2 cm,
- the inlet volumetric flow rate of the electrolyte ranged from 10 GPD to 100 GPD,
- the boundary condition on the cell is a constant temperature boundary conditions of 400 K,
- the left and right edges of the boundary are set to be the electrode locations,
- the inlet temperature of the fluid was room temperature at 293.15 K,
- and fully devleoped (thermally and hydrodynamically) laminar flow.

With this model, I was able to predict voltage, current, and power output with respect to flow rate. I was also able to predict the heat transfer coefficient of the cell.

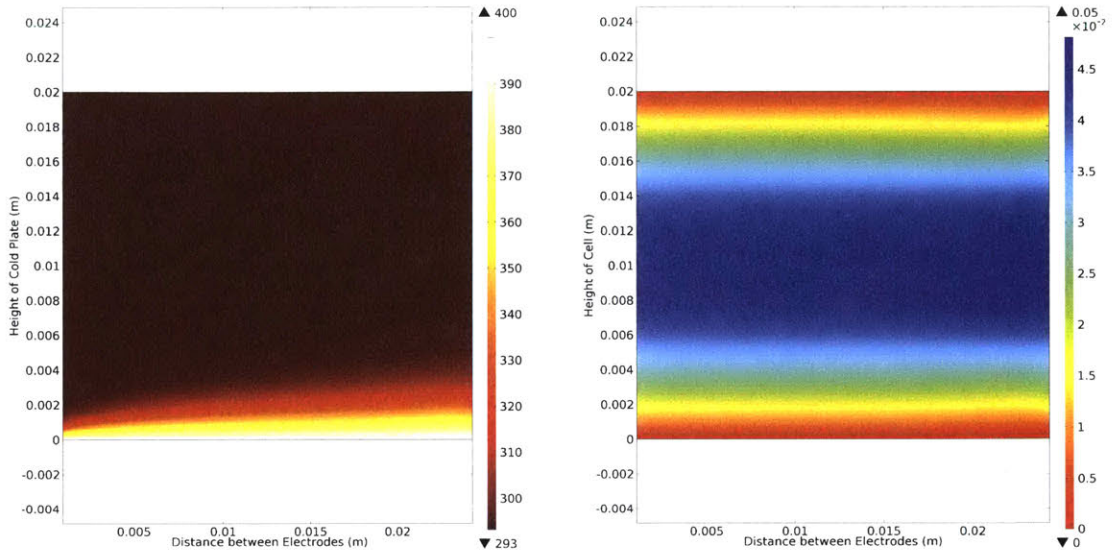

(a) *Temperature Profile* (b) *Velocity Profile*

Figure 4-2: (a) The steady state fully developed two dimensional temperature profile within the electrolyte under a constant temperature boundary condition. (b) The steady state lfully developed two dimensional laminar velocity profile of the electrolyte.

4.1.2 Results

The constant temperature boundary condition is the driver of the chemical reaction at the electrodes. Numerically, we can see the two-dimensional temperature distribution in a flowing electrolyte at steady-state, as well as the velocity profile of the electrolyte at steady-state in **fig. 4-2a & 4-2b**. The electrolyte obtains a maximum temperature increase to approximately the temperature of the boundary, while temperature diffuses inward. Clearly, the electrolyte has a parabolic velocity profile of the non-dimensional form:

$$\tilde{v}(y) = \left(1 - \frac{y^2}{h^2}\right), \tag{4.1}$$

where y is the distance from the centerline of the "differential" element, and h is the total height of the element. We should note that the heat flux imposed by the constant temperature boundary condition does not diffuse that far into the element itself.

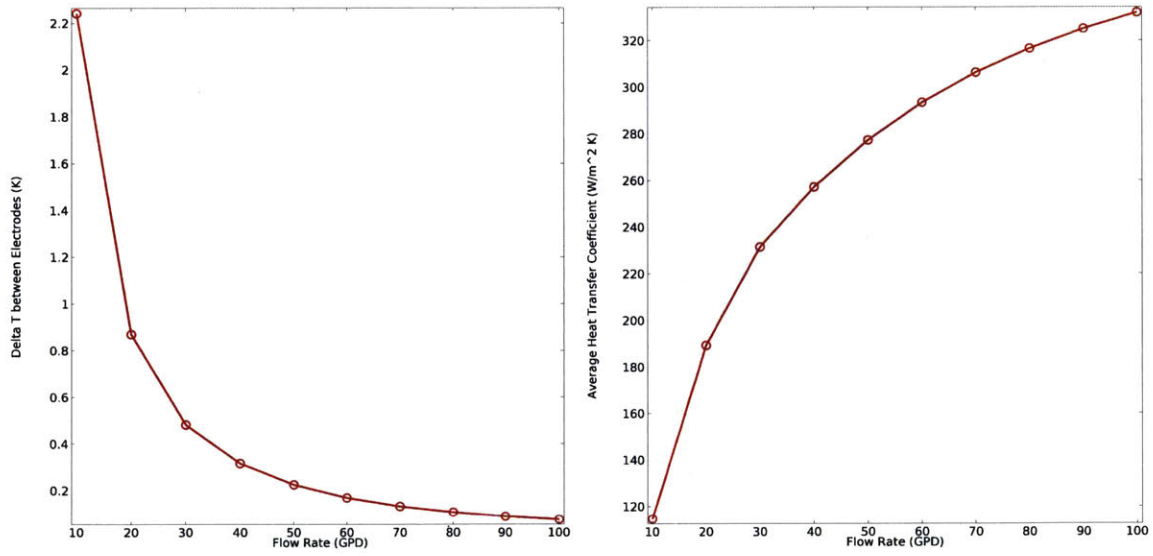

(a) *Inlet/outlet temperature difference vs. Flowrate* (b) *Heat Transfer Coefficient v. Flowrate*

Figure 4-3: (a) The inlet/outlet temperature difference as a function of the flow rate. As we expect, the difference decays exponentially as the flow rate increases. (b) The heat transfer coefficient as a function of flow rate. As expected, we see a higher heat transfer coefficient with increasing flow rate.

Power Generation

With the knowledge of the temperature distribution of the fluid, we can readily calculate how the inlet/outlet temperature difference varies with the flow rate. I had many options as to what spatial coordinate I would select to evaluate the temperature. I selected the midline of the "differential" element as the point to evaluate inlet and outlet temperature since this is the point, within my experiments, to which my electrodes reach when embedded in the top plate of the fTEC cell. As we can see in **fig. 4-3a** the maximum temperature difference of the inlet and outlet of the fluid is $\Delta T = 2.2$ K. Since the electrolyte I was using has a Seebeck coefficient of $S_e = 1.5$ mV/K then we expect that the maximum $V_{oc} = \Delta T S_e = 3.3$ mV. The V_{oc} as a function of flow rate is plotted in **fig. 4-4a**. As the flow velocity increases the temperature at the inlet and outlet will decrease. Therefore since the voltage output is proportional to the difference in inlet/outlet temperature, we expect the voltage output to decrease with increasing flow rate.

I also determined the short-circuit current as a function of the flow rate. Its trend follows a similar decay as the open-circuit voltage. As the flow rate increases, there is less time for each ion

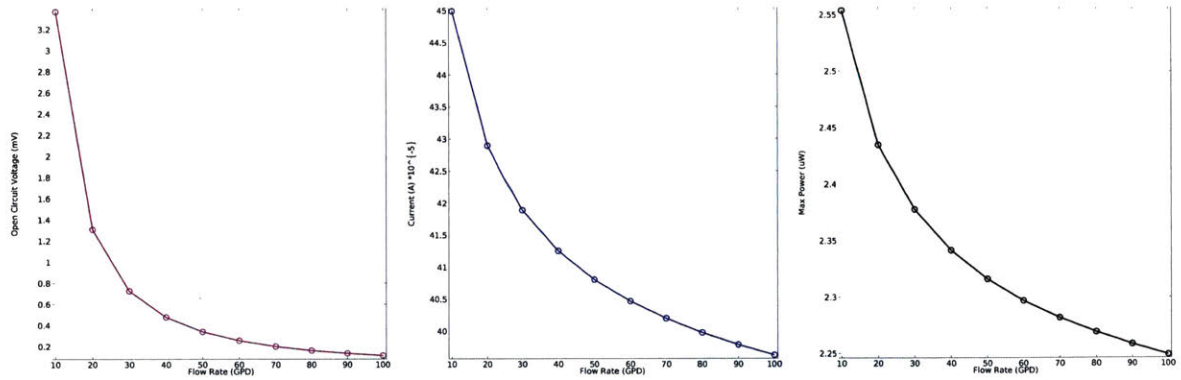

(a) *Voltage vs. Flowrate* (b) *Current vs. Flowrate* (c) *Power vs. Flowrate*

Figure 4-4: (a) The voltage output of the cell decreases as flow rate increases, indicative of a lower temperature difference between the inlet and the outlet. (b) The current output of the cell decreases as flow rate increases, indicative of less time for ions to interact with the electrode surfaces and exchange electrons. (c) The power output of the fTEC cell as a function of flow rate. The maxumim power output I numerically observed was $P_{max} = 2.55\ \mu$W.

to interact with the electrodes and transfer electrons to an external circuit. As a result, we expect the current to decrease with increasing flow rate. The behavior can be seen in **fig. 4-4b**. Now knowing both voltage and current I can determine the power output of the cell as a function of the flow rate. The maxumim power output I numerically observed was $P_{max} = 2.55\ \mu$W, as seen in **fig. 4-4c**.

Heat Transfer

The heat transfer coefficient is a good metric to evaluate the effectivness of the fTEC cell as a heat exchanger. With a constant temperature boundary condition, and knowledge of the inlet/outlet temperatures and the boundary condition temperature, we can use **eq. 2.27** to calculate the heat transfer coefficient. The heat transfer coefficient as a function of flow rate is plotted in **fig. 4-3b**. Clearly as the flow rate increases, the heat transfer coefficient increases, thus confirming our observation that power generation and heat transfer capabilties are at odds with each other. Numerically we observe a maximum heat transfer coefficient of approximately 340 W/m^{2}K.

This numerical analysis served as a solid basis on which I could evaluate (and validate) my physical fTEC cell, by comparing these results to my experimental results.

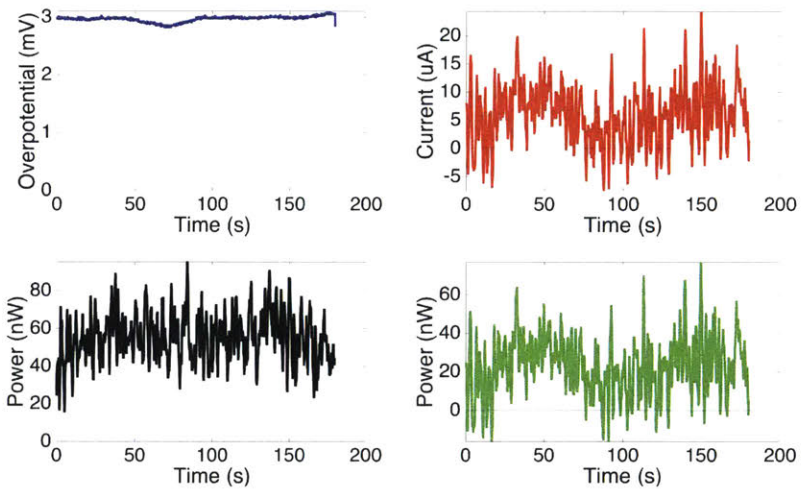

Figure 4-5: The first set of experiments where I recorded the voltage, current, and power outputs of the fTEC cell versus time. I recorded a $\Delta T = 2$ K which corresponds correctly to a voltage output of $V_{oc} = 3$ mV. However, the current and power outputs do not correspond well to the values I acheived numerically. This meant that something was wrong with my experimental setup.

4.2 Experimental Results

I experimentally determined the voltage, current, and power outputs for the fTEC cell as a function of the flow rate. I also determined the heat transfer coefficient of the fTEC cell for different flow rates. I first tested the cell using deionized water to ensure that all outputs were zero. After doing so I embarked on my first set of experiments.

For consistency between my numerical and physical experiments, I evaluated these temperature and electrical outputs of the fTEC cell only between two adjacent electrodes. Following the procedure outlined in **chapter 3**, I captured all of my electrical output data using a potentiostat, and the temperature data using a hand held thermocouple meter.

The first set of experiments were quite inconsistent. Between two electrodes I recorded a $\Delta T = 2$ K and a voltage, power, and current output that corresponds to **fig. 4-5**. Clearly the voltage output corresponds well to $V_{oc} = \Delta T S_e$, but the current and power outputs do not correspond well. This informed me that there was something wrong with my experimental setup. At this point in the project I started a collaboration with a 4^{th} PhD sutdent at Georgia Tech, Ali Kazim who is one of Professor Baratunde Cola's students, who developed a similar setup to mine. Note here that all data obtained and analyzed by Kazim is owned by him and I am simply referencing his

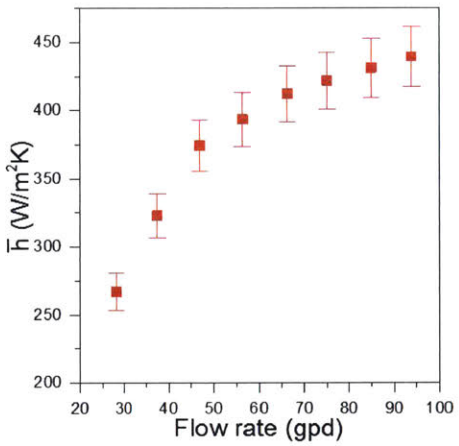

Figure 4-6: The heat transfer coefficient of the differential element as a function of the flow rate, obtained by Kazim. As we see, as the the flow rate increases, the heat transfer coefficient increases, indicating a greater ability to convect heat from a source.

results for this work. Both of our setups can be seen in **fig. 4-7 & 3-3b**. After a long discussion we determined that the reason for the erroneous outputs was due to the fact that my fTEC cell was not anodized. The process of anodization creates a thin non-conductive oxide layer on the aluminum thereby removing the possibility for the cell to short-circuit. Without this thin non-conductive layer, the cell would develop a short-circuit whereby the electrons transferred by the ions prefer a path of least resistance which is found simply by entering into any part of the aluminum cell. This is not the behavior that I wanted, especially when measuring the short-circuit current. I wanted the electrons to travel into the graphite electrodes and into the potentiostat for measurement.

Kazim had his fTEC cell anodized and he ran the same experiments and we were able to obtain the following outputs of the cell, **fig. 4-8**. Kazim was able to also test how different molarities of the electrolyte affected the voltage, current, and power outputs. From this second set of experimentation, we determined that the maximum $V_{oc} = 16$ mV, $I_{sc} = 50 \cdot 10^{-5}$ A, and $P_{max} = 2.0$ μW. He also determined that different molarities of the electrolyte only affected the current output since a higher molarity implies that there is a higher amount of ions that are readily available to transfer electrons to the electrode surfaces.

The experimentally determined heat transfer coefficient is shown in **fig. 4-6**. We note that the highest heat transfer coefficient measured was approximately 450 W/m^{2}K.

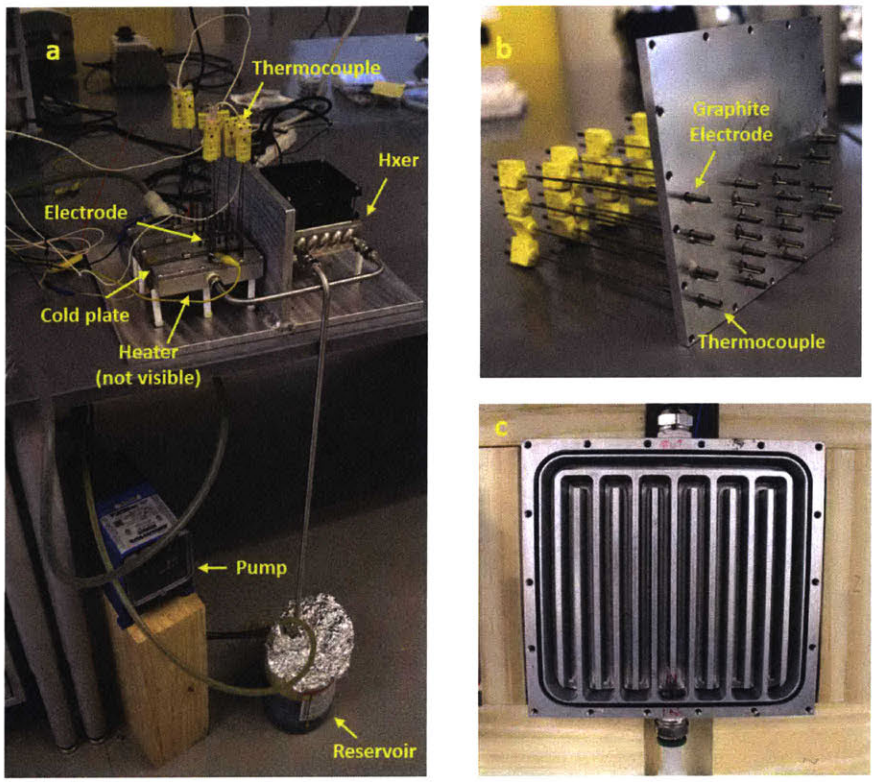

Figure 4-7: Kazim's setup for the fTEC cell, using a setup similar to my setup.

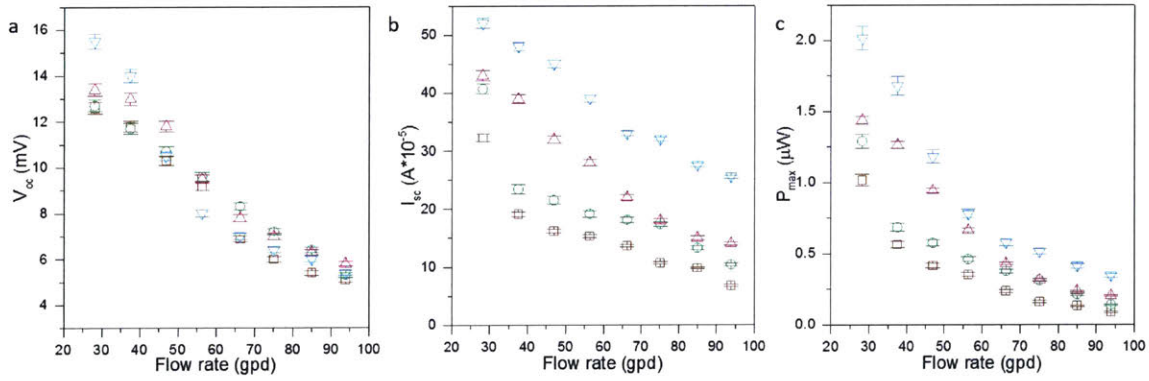

Figure 4-8: Results obtained using Kazim's setup, we can see a clear decay in the (a) voltage, (b) current, and (c) power output as the flow rate increases.

4.3 Discussion

In general, the numerical results for the "differential" element of the fTEC cell agree quite well with the experimental results. The difference for the maximum voltage, current, and power output is 12.6 mV, $7{\cdot}10^{-5}$ A, and 0.55 μW between the experimental results and the numerical results, and 100 W/m^{2}K for the heat transfer coefficient. For the voltage outputs, I can clearly see that the temperature dictates the voltage output and that at a higher temperature there is a higher voltage output. For the numerical results, however, I observe a lower voltage output for the given geometry than I see for the experimental voltage output. I believe this is the case since the electrolyte in the experimental cell is not guaranteed to undergo laminar flow, if there is any mixing or turbulence then there is a definite higher heat transfer coefficient and consequent temperature difference between electrodes. Secondly, in the actual fTEC cell, voltage is built up along entire surface of the electrode whereas within the numerical domain, the voltage is calculated at a point. However, the exponential decay is consistent between experimental and numerical results. The current and power values are quite similar and attain maximal values at low flow rates. The heat transfer coefficient, both numerically and experimentally, follow a similar trend as a function of flow rate both within the same order of magnitude of each other. A similar argument can be applied to understand the discrepancy between the two heat transfer coefficient values: the unknown nature of the flow regime for the experimental setup. All told, these results are suggestive that the device has been properly tested experimentally and evaluted numerically.

Chapter 5

Device Applications & Future Research Directions

For most of history, scientific research was brought about by a real world problem that society has faced. This thesis is no different. Waste-heat is prevalent in numerous places, as discussed in **chapter 1**, just waiting to be harvested and removed. This fTEC cell can potentially serve that purpose.

5.1 Data Centers

There is an inherent motivation to decrease the amount of electricity used by data centers, since the amount of electricity consumed has a direct relationship to the amount of carbon emissions (97 million metric tons in the current case) and cost of business operation. The main driver behind the need for so much electricity bases itself on the fact that CPUs, performing large amount of computations, produce a lot of thermal energy, and this thermal energy must be removed from the CPU to avoid component failure. Nowadays, half of the energy consumed in data centers is used to provide cooling to these CPUs in order to operate current infrastructure in a manner that avoids catastrophic electrical component failure. In an attempt to alleviate the low efficiencies of cooling technologies, liquid cooling has emerged as a viable method, compared to air cooling. By introducing an fTEC cell to current liquid cooling infrastructure we could supplement and augment existing cooling with the ability to harvest usable electrical energy. The demand for

cooling and energy harvesting technologies is likely to increase as a result of higher density CPU chips, hence methods to improve thermal management and increase power production will help to reduce our carbon footprint and save money.

5.1.1 Cost Analysis

I was curious as to what sort of cost savings a typical data center would incur if they implemented the fTEC cell that we developed and tested (assuming maximal power output from the cell). First we made the following assumptions:

- power produced per fTEC cell is $P_{max} = 2.2\ \mu$W per electrode pair,
- 44 electrode pairs per fTEC cell,
- each server in a data center utilizes 8-16 core 52×45 mm^2 CPUs,
- there are 30 servers per rack,
- each rack has a physical footprint of 11 ft^2,
- the data center is 100,000 ft^2.

From these assumptions we found that we can produce 1.147 mW/CPU and a power density of 25.05 mW/ft^2. As a result, for a 100,000 ft^2 facility, we can generate 2.505 kW of power.

Now we can determine the total cost savings as a result of this power output. If the same data center operates 24/7 for a whole year then we can generate about 21,958.26 kWh of energy per year. At a cost of about 0.20 \$/kWh we can save about \$4391.67 . This is a modest amount of money that most plant managers would surely pass up if it meant not needing to upgrade the entirety of the data center infrastructure. Therefore if we ever care to see this technology implemented, then the power output should be much higher.

5.2 Device Improvements

While developing the fTEC cell we noted the temperature dependence of the voltage output. One night I awoke after a dream and realized that if I wanted to maximize my voltage output I would need to place the electrodes in locations where ΔT is maximized. In the current configuration,

this occurs when one electrode is in the top plate and one electrode is directly below it, in the botom plate. We ran a quick COMSOL model to determine how well this would perform. The preliminary results suggest that we can attain a power output that is almost 3x the power output of the current deisgn.

While it may not be the most efficient, in its current form, there are numerous improvements that could be made to maximize the fTEC cell's performance. It would be interesting to see how higher surface area materials, such as carbon nanotubes, affect the outputs of the cell, as studied in [14]. This improvement, incorporated with the modified electrode placement could result in a fTEC cell that is commercially viable.

Bibliography

[1] Ocean Thermal Energy Conversion: An Overview. Technical report, NREL, 1989.

[2] Combined heat and power, waste heat, and district energy. Technical report, U.S. Department of Energy, 2011.

[3] Americas Data Centers Are Wasting Huge Amounts of Energy. Technical report, Natural Resources Defense Council, 2014.

[4] Sami Alkharabsheh, John Fernandes, Betsegaw Gebrehiwot, Dereje Agonafer, Kanad Ghose, Alfonso Ortega, Yogendra Joshi, and Bahgat Sammakia. A Brief Overview of Recent Developments in Thermal Management in Data Centers. *Journal of Electronic Packaging*, 137(4):40801, 2015. http://electronicpackaging.asmedigitalcollection.asme.org/article.aspx?doi=10.1115/1.4031326

[5] Enrico Barbier. Geothermal energy technology and current status: an overview. *Renewable and Sustainable Energy Reviews*, 6(1):3–65, 2002.

[6] Kasper A. Borup, Johannes de Boor, Heng Wang, Fivos Drymiotis, Franck Gascoin, Xun Shi, Lidong Chen, Mikhail I. Fedorov, Eckhard Müller, Bo B. Iversen, and G. Jeffrey Snyder. Measuring thermoelectric transport properties of materials. *Energy Environ. Sci.*, 8(2):423–435, 2015. http://xlink.rsc.org/?DOI=C4EE01320D

[7] E Bouty and E Bouty. Phenom electriques et electro-thermiques au contact d ' un m etal et d ' un liquide To cite this version :. *J. Phys. Theor. Appl*, 9(1):229–241, 1880. https://hal.archives-ouvertes.fr/jpa-00237647

[8] Olga Bubnova, Zia Ullah Khan, Abdellah Malti, Slawomir Braun, Mats Fahlman, Magnus Berggren, and Xavier Crispin. Optimization of the thermoelectric figure of merit in the conducting polymer poly (3 , 4-ethylenedioxythiophene). *Nature Materials*, 10(6):429–433, 2011. http://dx.doi.org/10.1038/nmat3012

[9] Brian N. (University of Western Australia) Figgis. Ligand Field Theory.

[10] H. K (Marlow Industries Inc.) Goldsmid. A simple technique for determining the Seebeck coefficient of thermoelectric materials. *J. Phys. E: Sci. Instrum.*, (19), 1986.

[11] a Gunawan, C H Lin, D a Buttry, V Mujica, R a Taylor, R S Prasher, and P E Phelan. Liquid Thermoelectrics: Review of Recent And Limited New Data of Thermogalvanic Cell Experiments. *Nanoscale and Microscale Thermophysical Engineering*, 17(4):304–323, 2013. %7B%3C%7DGo to

[12] Andrey Gunawan, Nicholas W Fette, and Patrick E Phelan. Thermogalvanic waste heat recovery system in automobiles. In *ASME 2015 Power Conference collocated with the ASME 2015 9th International Conference on Energy Sustainability, the ASME 2015 13th International Conference on Fuel Cell Science, Engineering and Technology, and the ASME 2015 Nuclear Forum*, pages V001T11A002—-V001T11A002. American Society of Mechanical Engineers, 2015.

[13] Toshiro Hirai, Kazuhiko Shindo, and Tsutomu Ogata. Charge and discharge characteristics of thermochargeable galvanic cells with an [Fe (CN) 6] 4-/[Fe (CN) 6] 3- redox couple. *Journal of the Electrochemical Society*, 143(4):1305–1313, 1996.

[14] Renchong Hu, Baratunde a Cola, Nanda Haram, Joseph N Barisci, Sergey Lee, Stephanie Stoughton, Gordon Wallace, Chee Too, Michael Thomas, Adrian Gestos, Marilou E Dela Cruz, John P Ferraris, Anvar a Zakhidov, and Ray H Baughman. Harvesting waste thermal energy using a carbon-nanotube-based thermo-electrochemical cell. *Nano letters*, 10(3):838–846, mar 2010. http://www.ncbi.nlm.nih.gov/pubmed/20170193

[15] Tae June Kang, Shaoli Fang, Mikhail E Kozlov, Carter S Haines, Na Li, Yong Hyup Kim, Yongsheng Chen, and Ray H Baughman. Electrical Power From Nanotube and Graphene Electrochemical Thermal Energy Harvesters. *Advanced Functional Materials*, 22(3):477–489, feb 2012. http://doi.wiley.com/10.1002/adfm.201101639

[16] Hee Seok Kim, Weishu Liu, Gang Chen, Ching-Wu Chu, and Zhifeng Ren. Relationship between thermoelectric figure of merit and energy conversion efficiency. *Pnas*, 112(27):8205–10, 2015. http://www.pnas.org/content/112/27/8205.abstract

[17] Kent B Koller and Fred M Hawkridge. Temperature and electrolyte effects on the electron-transfer reactions of cytochrome c. *Journal of the American Chemical Society*, 107(25):7412–7417, 1985.

[18] Renee Kroon, Desalegn Alemu Mengistie, David Kiefer, Jonna Hynynen, Jason D. Ryan, Liyang Yu, and Christian Müller. Thermoelectric plastics: from design to synthesis, processing and structurefi?!property relationships. *Chem. Soc. Rev.*, pages 6147–6164, 2016. http://xlink.rsc.org/?DOI=C6CS00149A

[19] G I Meijer. Cooling energy-hungry data centers. *Science*, 328:318–319, 2010.

[20] A J Minnich, M S Dresselhaus, Z F Ren, and G Chen. Bulk nanostructured thermoelectric materials : current research and future prospects. pages 466–479, 2009.

[21] Y Mua and Quickenden. Power Conversion Efficiency, Electrode Separation, and Overpotential in the Ferricyanide/Ferrocyanide Thermogalvanic Cell. *Journal of The Electrochemical Society*, 143(8):2558, 1996.

[22] Bed Poudel, Qing Hao, Yi Ma, Yucheng Lan, Austin Minnich, Bo Yu, Xiao Yan, Dezhi Wang, Andrew Muto, Daryoosh Vashaee, and Others. High-thermoelectric performance of nanostructured bismuth antimony telluride bulk alloys. *Science*, 320(5876):634–638, 2008.

[23] T I Quickenden and Y Mua. A Review of Power Generation in Aqueous Thermogalvanic Cells. *Journal of Electrochemical Society*, 142(11):3985–3994, 1995.

[24] D M Rowe and Fundamental Concepts. General Principles and Basic Considerations. In *Thermoelectrics Handbook*, pages 1–14. CRC Press, dec 2005. http://dx.doi.org/10.1201/9781420038903.sec1

[25] Pablo F Salazar, Satish Kumar, and Baratunde a. Cola. Nitrogen- and Boron-Doped Carbon Nanotube Electrodes in a Thermo-Electrochemical Cell. *Journal of The Electrochemical Society*, 159(5):B483, 2012. http://jes.ecsdl.org/cgi/doi/10.1149/2.043205jes

[26] Pablo F Salazar, Satish Kumar, and Baratunde a. Cola. Design and optimization of thermo-electrochemical cells. *Journal of Applied Electrochemistry*, 44(2):325–336, oct 2013. http://link.springer.com/10.1007/s10800-013-0638-y

[27] Thomas Johann Seebeck. Ueber die magnetische Polarisation der Metalle und Erze durch Temperaturdifferenz. *Annalen der Physik*, 82(3):253–286, 1826.

[28] G Jeffrey Snyder and Eric S Toberer. Complex thermoelectric materials. *Nature materials*, 7(2):105–114, 2008.

[29] Ingo Stark. Invited talk: Thermal energy harvesting with Thermo Life. In *International Workshop on Wearable and Implantable Body Sensor Networks (BSN'06)*, pages 19–22. IEEE, 2006.

[30] Thad Starner. Human-powered wearable computing. *IBM systems Journal*, 35(3.4):618–629, 1996.

[31] J. Tan. Thermoelectric properties of bismuth telluride thin films deposited by radio frequency magnetron sputtering. *Proceedings of SPIE*, 5836(July 2005):711–718, 2005. http://link.aip.org/link/?PSI/5836/711/1&Agg=doi

[32] Maria Telkes. Solar thermoelectric generators. *Journal of Applied Physics*, 25(6):765–777, 1954.

[33] Cronin B Vining. An inconvenient truth about thermoelectrics. *Nature materials*, 8(2):83–85, feb 2009. http://www.ncbi.nlm.nih.gov/pubmed/19165205

[34] Hainan Zhang, Shuangquan Shao, Hongbo Xu, Huiming Zou, and Changqing Tian. Free cooling of data centers: A review. *Renewable and Sustainable Energy Reviews*, 35:171–182, 2014.